*Proceedings of 7th Transport Research Arena TRA 2018, April 16-19, 2018, Vienna, Austria*

# Thermal runaway and battery fire: comparison of Li-ion, Ni-MH and sealed lead-acid batteries

Andrey W. Golubkov[a]*, Rene Planteu[a], Bernhard Rasch[a], Christiane Essl[a], Alexander Thaler[a], Viktor Hacker[b]

[a] *VIRTUAL VEHICLE Research Center, Inffeldgasse 21a, 8010 Graz, Austria*
[b] *Institute of Chemical Engineering and Environmental Technology - Graz University of Technology, Inffeldgasse 25/C/II, 8010 Graz, Austria*

**Abstract**

Rechargeable batteries are a key component for sustainable mobility. The last years showed a significant reduction of price and increase in energy density of Li-ion batteries for electric vehicles. Unfortunately, batteries with high energy density can be source of hazard. Recently, burning Li-ion batteries of mobile-phones got a lot of negative attention in the media.
In the first part of the paper we review the hazards of conventional Ni-MH and sealed lead-acid batteries. In the second part we focus on Li-ion batteries: we introduce different cell geometries and electrode types, we show a test-stand designed to measure thermal runaway characteristics in our laboratory and finally we conclude with results of a real thermal runaway experiment.

*Keywords:* Li-ion batteries; thermal runaway; battery fire; battery safety; electric vehicles

* Corresponding author. Tel.: +43 (316) 873 - 9639
*E-mail address:* andrej.golubkov@v2c2.at

**Nomenclature**

| | |
|---|---|
| AGM | absorbed glass mat battery (lead acid) |
| DCA | dynamic charge acceptance (of lead acid batteries) |
| EFB | enhanced flooded battery (lead acid) |
| ICE | internal combustion engine |
| LCO | $LiCoO_2$, cathode material for Li-ion batteries |
| LFP | $LiFePO_4$, cathode material for Li-ion batteries |
| LMO | $LiMn_2O_4$, cathode material for Li-ion batteries |
| LTO | $Li_4Ti_5O_{12}$, anode material for Li-ion batteries |
| NMC | $Li(NiMnCo)O_2$, cathode material for Li-ion batteries |

## 1. Introduction

Electrified vehicles differ from conventional vehicles by utilizing electric energy for traction in addition or instead of an ICE engine. The electrified vehicles are categorized – with increasing battery size – in micro hybrid, 48V (mild hybrid) to full hybrids, plug-in vehicles (PHEV) and battery-electric vehicles (BEV) (Table 1). The later are fully electrified and have no ICE at all. Different type of battery technologies are utilized for different degrees of electrification. Advanced lead-acid batteries are used in micro hybrids, Ni-MH is predominantly used in full-hybrid vehicles from Toyota, and different types of Li-ion batteries are used for all ranges of electrification (Rosenkranz et al. 2016).

In this paper we discuss safety risks of those battery technologies: what can go wrong and what are the consequences. Electric shock hazard and fires risk from faulty electric connectors or electric drivetrain components are equally important but outside of the scope of this paper.

Table 1. Basic battery types for electrified vehicles (Fetcenko et al. 2015)

| | Advanced lead-acid | Ni-MH | Li-ion power optimized | Li-ion energy optimized |
|---|---|---|---|---|
| Applications | micro hybrid | micro hybrid, full hybrid | micro hybrid, full hybrid | PHEV, BEV |
| Energy density, cell level, Wh/kg | 40 | 50 - 110 | 50 -100 | 250 |
| Power density, cell level, W/kg | 450 (at -18°C) | 1500 | up to 4000 | 400 |

## 2. Lead-acid batteries

Prolonged charging at high temperatures can cause a thermal runaway of valve regulated EFB and AGM batteries. The thermal runaway is caused by reactions which accelerate each other: high temperature, water loss from electrolysis, increased exothermal oxygen recombination, further temperature increase, increase of the float current and again temperature increase (Fig. 1). Eventually the plastic casing may soften and battery temperature can reach the boiling temperature of the electrolyte. If the overpressure valve fails, the battery casing will expand under hydrogen-gas pressure and the battery will pose a significant risk of gas deflagration and spill of sulfuric acid electrolyte. To avoid chances of thermal runaway easily observable parameters like temperature, electrical resistance or voltage fluctuation due to arcing should be monitored. If an anomaly is detected, the power should be reduced (Rand et al. 1996).

Advanced lead-Acid batteries for micro hybrid systems incorporate carbon additives (Karden 2017) or carbon grid structure (McKenzie 2017) in the negative plate to improve charge kinetics. Unfortunately this increases the risk of $H_2$ production: there is a trade-off between improved DCA (through carbon material) and $H_2$ evolution during charge with high currents at high temperatures. The hydrogen may accumulate inside the battery pack where it may cause explosion hazard. Good venting or gas monitoring is needed.

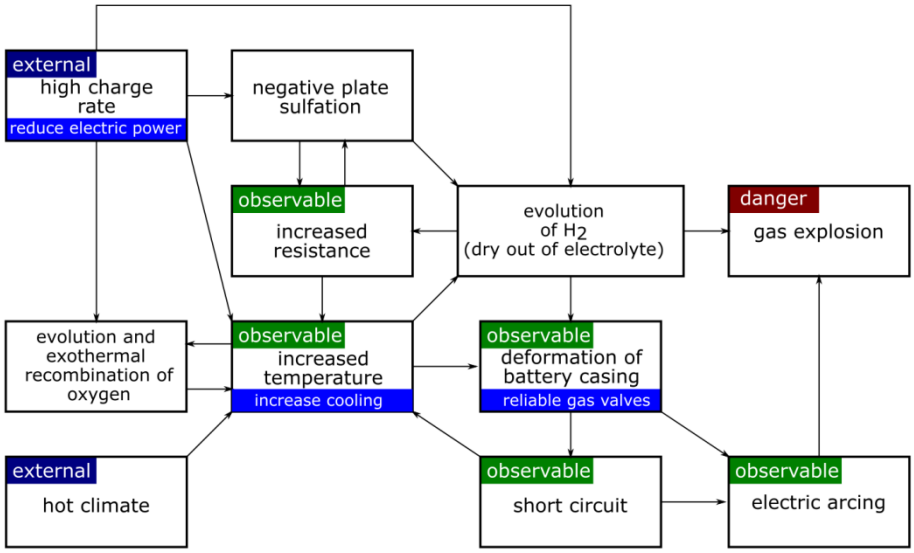


Fig. 1 Thermal runway mechanism and mitigation options of valve regulated lead acid batteries

## 3. Ni-MH batteries

Nickel metal-hydride (Ni-MH) batteries are being used since 1997 in hybrid cars and there is still little literature on their safety (Fetcenko et al. 2015). This indicates that there seems to be few known safety issues with this type of batteries. Similar to lead acid batteries, Ni-MH batteries can produce $O_2$ during overcharge and at temperatures > 40°C. An effective countermeasure is incorporation of oversized negative electrodes and LiOH additives which enable $O_2$ and $H_2$ recombination during charge and overcharge. Large cells incorporate valves to prevent excessive gas pressure build-up.

## 4. Li-ion batteries

Most literature on battery safety deals with Li-ion batteries. Safety risks are caused by their high energy density, the high cell voltages and the inflammable electrolyte. In Li-ion batteries a small local failure can grow to a full thermal runaway. This can be pictured like bursting of a dam which starts with a small trickle and then quickly evolves into a full breach. Unlike to the thermal-runaway of a lead acid battery, a thermal runaway of a Li-ion battery can easily cause battery fire. Before we go into detail of failure modes, we need to explain the different types of Li-ion batteries.

### *4.1. Types of Li-ion batteries*

Li-ion battery-cells can have different casings, different sizes and different anode/cathode combinations (Zhang & Ramadass 2012). They can be either optimized for high power-density or high energy-density. Common cell-casings are small cylindrical metal cans, bigger prismatic metal cans and so called pouch cells (Fig. 2). The casings of metal cans are made by deep drawing from stainless steel or aluminium. The casings of pouch cells are made of composite aluminium-plastic foils.

Most common cylindrical cells have a diameter of 18 mm and a length of 65 mm. Their capacity ranges from 1 to 3.5 Ah. They are mostly used for consumer electronics, power tools and electric bikes. Tesla is the only car manufacturer who utilises 18650 cells in mass produced electric cars. Prismatic metal-can cells for automotive applications have capacities ranging from 5 to 120 Ah. The smaller cells are used for hybrid cars and the bigger ones are used in battery packs for pure electric vehicles. Small pouch cells are found in consumer electronics such as notebooks or mobile phones, bigger pouch cells with capacities up to 90 Ah are used in battery packs of electric vehicles. It is not yet clear if pouch cells or metal-can cells will dominate in battery packs of future electric vehicles. Pouch cells have cheaper and lighter casings but prismatic metal-can cells have better mechanical properties and are easier to cool.

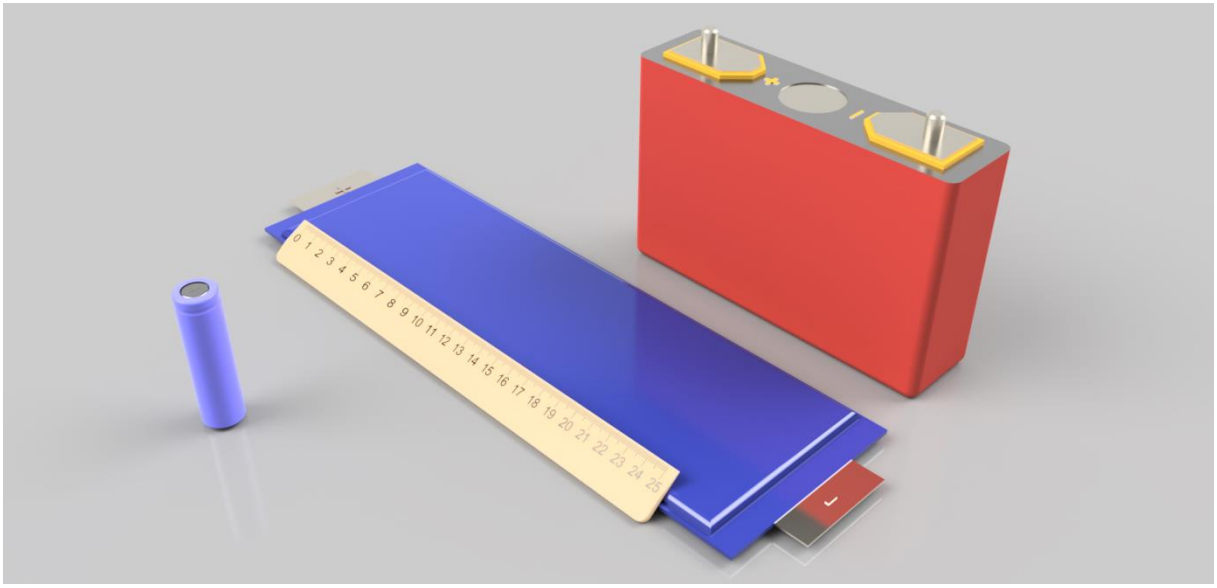

Fig. 2 Different sizes and casings of Li-ion battery-cells. From left to right: cylindrical metal-can, pouch cell, prismatic metal-can

All commercial Li-ion cells have the same basic elements inside their casings: thin metal foils which are thickly coated with electrochemically active cathode or anode material and separator layers are either stacked or rolled and soaked with Li-ion conducting electrolyte. The metallic foils are electrically connected to the outside terminals (Fig. 3).

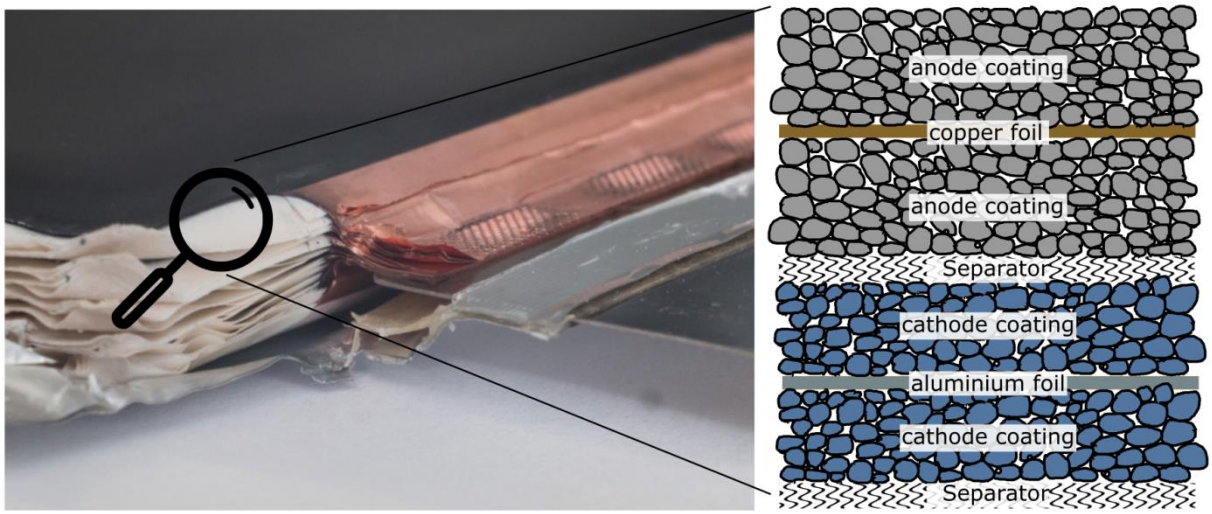


Fig. 3 (left) Photograph of a pouch cell with removed casing and revealed layer structure. Extensions of the copper foils are connected to the negative terminal. (right) Sketch of one repeating unit of the layer structure

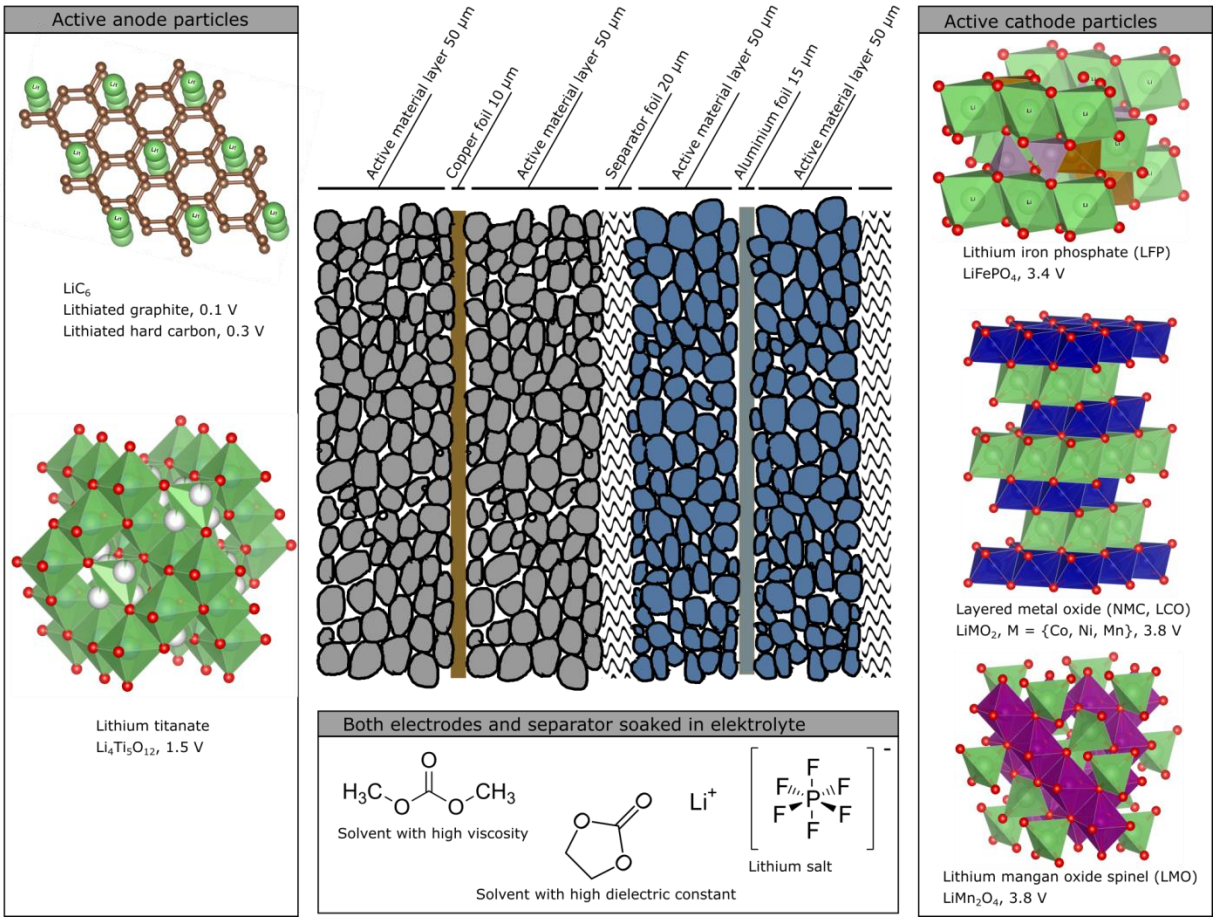


Fig. 4 (left) Typical choices for electrochemically active anode material. (centre) Typical thicknesses of the layers. (Right) Typical choices for electrochemically active cathode material. (Bottom) commercially used electrolyte components. The voltages describe the mean potential of the materials vs $Li/Li^+$

Typical choices of electrode material are graphite particles for the anode and layered metal oxide particles such as $Li(NiMnCo)O_2$ (NMC) for the cathode. During cell production the particles are mixed with an conducting agent and a binder in a liquid solvent to form a so called slurry. The slurry is then coated on the respective metal foil and the solvent is removed by drying. The anode slurry is coated on copper foil and the cathode slurry is coated on an aluminium foil. The separator foil is placed between the electrodes. The layers are then either rolled or stacked and placed into the cell casing. The next steps are the filling of the electrolyte, the first charging of the cell and the final sealing of the cell casing.

The open circuit voltage (OCV) of the cell is the difference of the electrochemical potential of the two electrodes. In case of graphite (0.1 V vs. Li) and NMC (3.8 vs. Li) the mean OCV is 3.7 V. Such extreme electrochemical potentials require special electrolytes with specialized components. Typical cells use $LiPF_6$ as the lithium salt because it also helps to passivate the aliminium foil of the cathode. Ethylencarbonate (EC) is used as the solvent with high dipole moment to increase Li-salt concentration and also because it builds a Li-ion conducting passivation layer on top of the graphite particles (Xu 2004). Unfortunately, EC has high viscosity and dimethylcarbonate or diethylcarbonate are added to lower viscosity and to improve Li-ion conductivity at low temperatures. The stack structure and some alternative choices for anode and cathode material are shown in figure 4.

The power to energy ratio of Li-ion cells is determined by the type of electrode material, by the electrode porosity and by the thicknesses of the electrode coatings and metal foils (Table 2). Thicker coatings and lower porosity (higher compression during manufacturing) increase the cell capacity. Unfortunately, this also increases the path length for the Li-ions on their way from one electrode particle to the other thus limiting the electric power of the cell. High power cells have thinner coatings and higher porosity to decrease ionic resistance and thicker metal foils to decrease electric resistance. High power cells also may use special anodes like lithiumtitanate (LTO) or hard-carbon to improve fast charging because their electrochemical potential vs. lithium

allows for higher dynamic polarisation and current density before unwanted metallic lithium deposition happens on the anode (Zhao et al. 2015).

Table 2. Optimization options for Li-ion batteries

| | power optimized | energy optimized |
|---|---|---|
| Anode | LTO, hard carbon | graphite |
| Cathode | LFP, NMC, LMO | NMC, NCA |
| electrode porosity | 60% | 30% |
| thickness of electrode coatings | thin | thick |
| thickness of the metal foils | thick | thin |

### *4.2. Initial causes of cell failure*

The thermal runaway of a Li-ion cell is a chemical reaction, with a temperature higher than the *temperature of no return*, where the heating rate from the exothermal reaction is higher than the cooling rate by the adjacent components. A battery pack has several potential sources of unwanted initial heating (Larsson & Mellander 2014) which are able to exceed the temperature of no return:

- External sources like fire
- Bad electrical interconnectors with increased electrical resistance combined with high current
- Internal short circuits (foreign particles/objects, lithium dendrites from overcharge, copper dendrites from over-discharge)

The case of overcharge is complicated because several effects may take place simultaneously:

- Joule heating due to increased cell resistance
- Chemical destabilization of the cathode particles due to over-delithiation
- Deposition of reactive metallic lithium on the surface of the fully lithiated anode particles

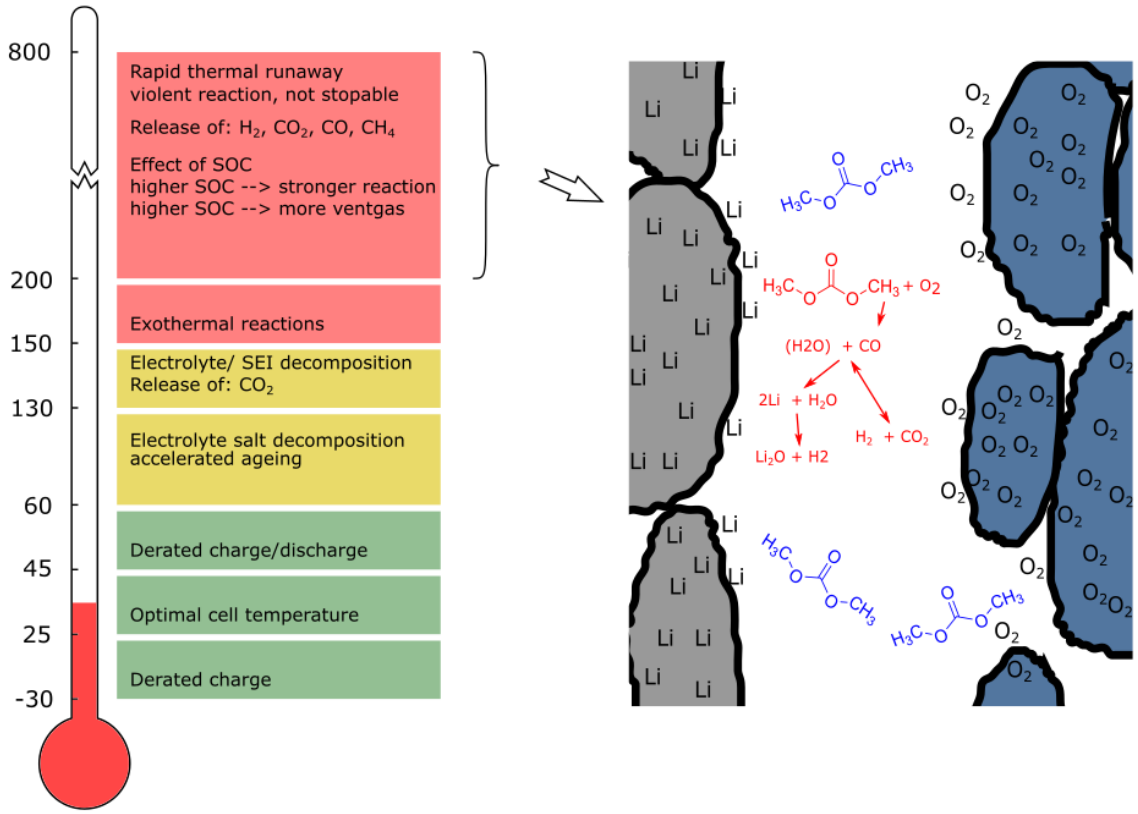


Fig. 5 (left) Sketch of thermal events for a Li-ion battery with energy density above 200 Wh/kg. (right) Main thermal runaway reactions

### *4.3. Single cell failure*

Figure 5 shows the effects of temperature on a charged (or overcharged) Li-ion cell. Normal operating temperatures lie between -30°C and 60°C. To prevent excessive ageing, the battery management will derate the power below 10°C and above 45°C. Above 60°C the battery will be completely disconnected to prevent Li-salt decomposition. Above 130°C the SEI and electrolyte will decompose and release $CO_2$ (Lammer et al. 2017). Above 150°C reactions will become exothermal and the cell will go into rapid thermal runaway above 200°C.

The main thermal-runaway reactions are combustion of electrolyte with oxygen which is released by the metal-oxide cathode and oxidation of the lithium which is released by the graphite anode. The amount of both released ingredients – lithium and oxygen – is directly proportional to the stored energy of the Li-ion cell. A fully charged cell will release the complete amount of Li and $O_2$ while a fully discharged cell will neither release any Li nor $O_2$. Overcharged cells release even more Li and $O_2$. Similarly, a cell with high capacity will release more Li and $O_2$ than a cell with low capacity. Consequently, a charged cell with high energy density shows a more severe thermal runaway reaction compared to a not fully charged cell or a cell with low energy density.

The main components of released gas are CO and $CO_2$ from oxygen starved combustion electrolyte, binder and separator and $H_2$ from lithium oxidation (Golubkov et al. 2015; Golubkov et al. 2014). The ratio of CO and $CO_2$ depends on the reaction temperature (Boudouard reaction). Temperatures above 700°C favour CO over $CO_2$.

### *4.4. Thermal runaway propagation*

In automotive battery packs cells are stacked as tight as possible to reduce pack volume. Typical numbers of cells in a battery pack range from 88 (PHEV) to 400 (BEV) in case of prismatic/pouch cells and 8000 (Teslas BEV) in case of small cylindrical cells. If one of those cells fails and transits into thermal runaway it will heat the adjacent cells. If the adjacent cells reach the critical temperature, they go into thermal runaway as well and the thermal runaway starts to propagate through the whole battery pack, eventually ending in a full battery fire. To prevent thermal runaway propagation, thermal barriers must be included between adjacent cells (Feng et al. 2015).

## 5. Experiment results, thermal runaway of large automotive Li-ion cells

### *5.1. Tested cell*

We did experiments with automotive prismatic cells with graphite anodes and LMO cathodes. The cell has a mass of 1.7 kg, a capacity of 50 Ah and a mean voltage of 3.6 V. The cell designs dates from 2009 and therefore the energy density is rather low with 105 Wh/kg if compared with up-to date cells.

### *5.2. Test method*

We developed a heavy-duty test rig to do experiments with large Li-ion cells. The test rig consists of a pressure tight reactor with a heatable sample-holder, many temperature sensors and a pressure sensor. Figure 6 shows the reactor in opened and closed state and figure 7 shows the sample holder.
In each experiment the cell is fully charged and placed into the sample holder. Subsequently the reactor is closed, evacuated and filled with nitrogen. Then the sample holder starts to heat the cell until a thermal runaway is detected. The test stand measures the cell-casing temperature, the gas temperature near the exit of the burst plate of the cell and the mean gas temperature in the reactor as well as the cell voltage and the gas pressure. The amount of released gas is calculated with the ideal gas law.

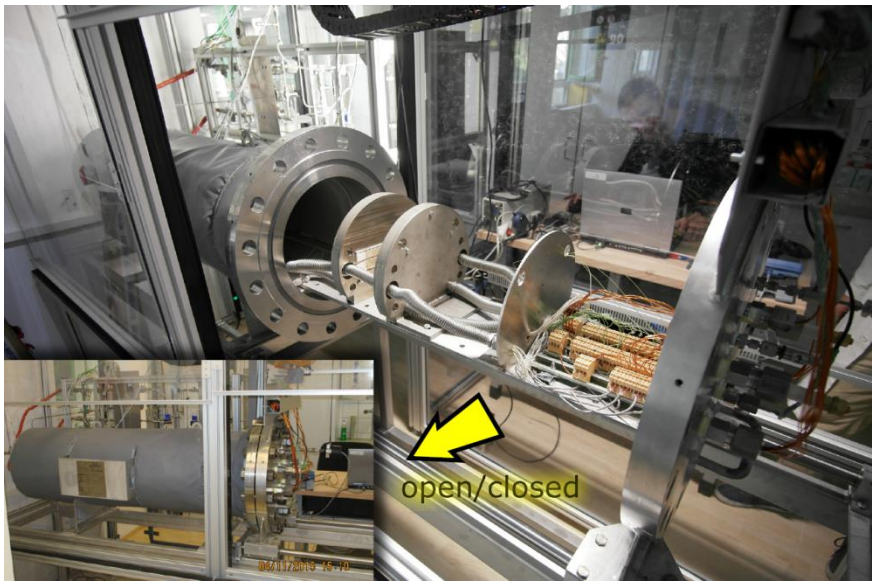


Fig. 6, Photograph of the thermal runaway test-stand. The main component is a massive gas-tight reactor, shown in opened and closed state

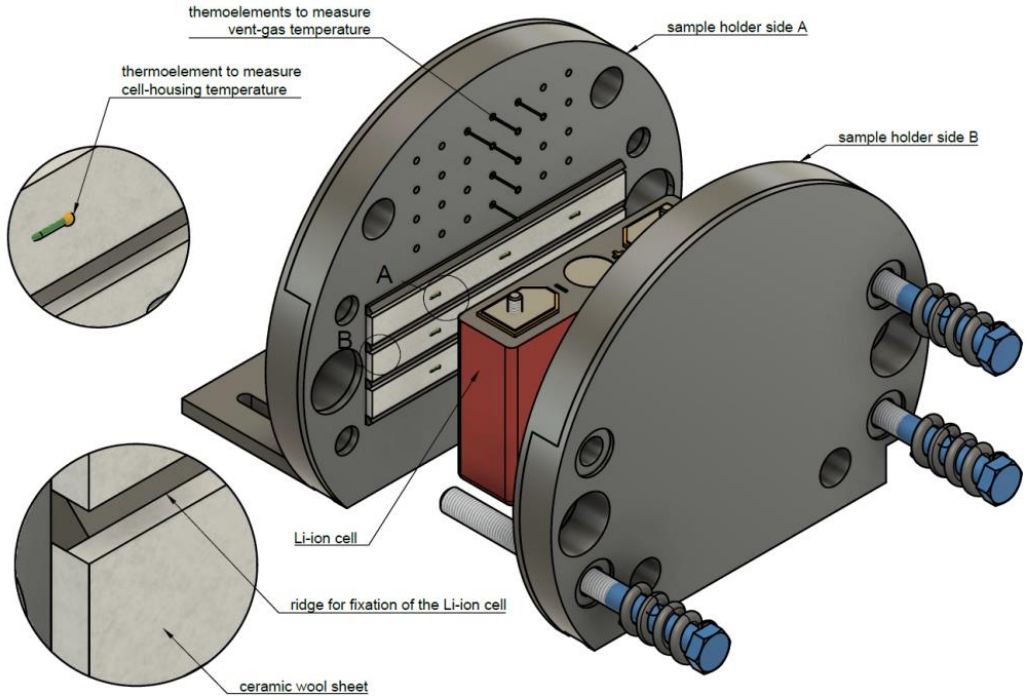


Fig. 7, Sketch of the sample holder for metal-can cells. The sample holder includes internal electric heating and a number of temperature sensors (thermocouples) to measure the cell surface temperature and the vent-gas temperature

### *5.3. Typical experiment outcome*

The sample was heated with a constant temperature rate (2.3 °C/min). The voltage of the cell collapsed from 4.08 to 0 V at 176 °C. The burst plate of the cell opened at a cell temperature of 205°C and released 0.36 mol of gas. After further heating, up to a cell temperature of 247°C, the cell transited into a rapid thermal runaway and at the same time a second venting occurred with a gas release of additional 2.8 mol. The cell reached a maximum temperature of 532°C during thermal runaway. The maximum recorded temperature of the vent-gas was 530°C measured directly above the burst plate of the cell. After the thermal runaway the heating of the sample holder was switched off and the cell cooled down subsequently (Fig. 8). The cell lost 35% of its mass during the experiment by ejecting gas and particles through its venting plate.

It is important to know the duration of the main thermal runaway reaction and how long it takes to emit the gas. The cell emits hot vent-gas as long as the rapid thermal runaway reaction takes place. Therefore we can assume

that the duration of the reaction is the same as the duration where vent-gas temperature sensors measure high temperature. In the temperature plot, the vent-gas sensors stay above 500°C for 2.7 s and so we assume 2.7 seconds as the duration. Alternatively, we can estimate the venting duration from the pressure plot. The representative time - the time the pressure needs to increase from the pressure level before the main reaction to the maximum pressure level - is equal to 3 seconds.

Now we can calculate the release rate of the vent-gas. By taking 3 seconds as release time and 2.8 mol as the amount of released gas we arrive at 0.9 mol/s. This is equal to 22 litre/s at standard temperature and pressure. The release rate can be further used to specify the venting system of the battery pack housing so that gases are emitted to the outside of the electric vehicle.

The maximum temperature and the onset temperature can be included in thermal runaway propagation models to specify the needed heat barriers between individual cells in the battery pack.

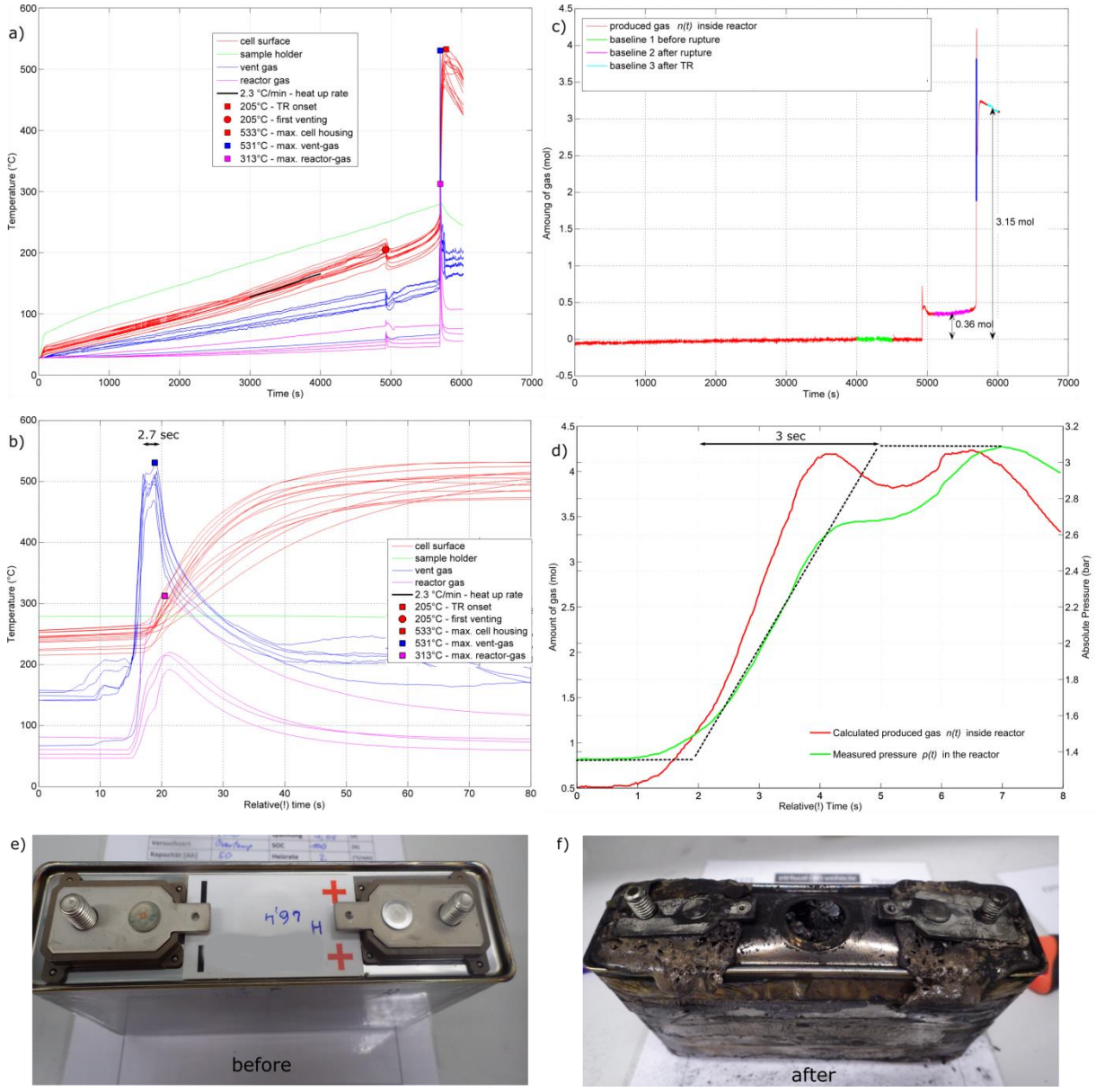


Fig. 8, (a) temperature of the cell casing, the vent-gas and the reactor-gas. Full experiment duration. (b) Detailed temperature plot showing only the main thermal runaway event. (c) Calculated amount of released gas inside the reactor. Full experiment duration. (d) Detailed pressure plot, showing only the main gas release. (e,f) Cell sample before and after the experiment.

## 6. Conclusion

In this paper we compared the safety of batteries for electrified vehicles. The thermal runaway of lead acid batteries batteries is driven by high charging current/voltage at high temperatures. It is easily detectable with temperature or gas sensors and can be mitigated by reducing the electric load. Ni-MH batteries show very good safety records. We could not find any literature on possible thermal runaway reactions of Ni-MH batteries.

The thermal runaway of Li-ion cells is initiated by overtemperature or overcharge. Their main thermal runaway reaction can be quite dramatic and can easily end with a battery fire. The severity of the Li-ion thermal-runaway reaction is proportional to the amount of electrochemical energy inside the cell. Cells with higher energy density reach higher maximal temperatures and release more vent-gas. Charged cells can go into thermal runaway but discharged cells show no thermal runaway reaction. In Li-ion battery packs special care must be taken to prevent hot-spots, foreign object intrusion, dendrites inside the cells and overcharge. Thermal barriers between the cells may be used to prevent thermal runaway propagation from cell to cell. Battery packs need proper gas venting (exhasut) systems so that in case of failure harmfull gases are directed to the outside of the vehicle.

## 7. Acknowledgements

This work was accomplished at the VIRTUAL VEHICLE Research Center in Graz, Austria. The authors would like to acknowledge the financial support of the COMET K2 - Competence Centers for Excellent Technologies Programme of the Austrian Federal Ministry for Transport, Innovation and Technology (bmvit), the Austrian Federal Ministry of Science, Research and Economy (bmwfw), the Austrian Research Promotion Agency (FFG), the Province of Styria and the Styrian Business Promotion Agency (SFG). They would furthermore like to express their thanks to their supporting industrial and scientific project partners, namely AVL List GmbH and to the Technical University Graz.

## 8. References

Feng, X. et al., 2015. Characterization of penetration induced thermal runaway propagation process within a large format lithium ion battery module. *Journal of Power Sources*, 275, pp.261–273. Available at: http://dx.doi.org/10.1016/j.jpowsour.2014.11.017.

Fetcenko, M., Koch, J. & Zelinsky, M., 2015. Nickel–metal hydride and nickel–zinc batteries for hybrid electric vehicles and battery electric vehicles. In *Advances in Battery Technologies for Electric Vehicles*. Elsevier, pp. 103–126. Available at: http://dx.doi.org/10.1016/B978-1-78242-377-5.00006-6.

Golubkov, A.W. et al., 2014. Thermal-runaway experiments on consumer Li-ion batteries with metal-oxide and olivin-type cathodes. *RSC Advances*, 4(7), p.3633. Available at: http://xlink.rsc.org/?DOI=c3ra45748f [Accessed December 20, 2013].

Golubkov, A.W. et al., 2015. Thermal runaway of commercial 18650 Li-ion batteries with LFP and NCA cathodes – impact of state of charge and overcharge. *RSC Adv.*, 5(70), pp.57171–57186. Available at: http://xlink.rsc.org/?DOI=C5RA05897J.

Karden, E., 2017. How Harmful Are Carbons in Enhanced Flooded Batteries for High Temperature Use Cases ? In *7th Advanced Automotive Battery Conference Europe*. Mainz, Germany: Advanced Power Supply and Energy Management Ford Research & Advanced Engineering Europe.

Lammer, M., Königseder, A. & Hacker, V., 2017. Holistic methodology for characterisation of the thermally induced failure of commercially available 18650 lithium ion cells. *RSC Adv.*, 7(39), pp.24425–24429. Available at: http://xlink.rsc.org/?DOI=C7RA02635H.

Larsson, F. & Mellander, B.-E., 2014. Abuse by External Heating, Overcharge and Short Circuiting of Commercial Lithium-Ion Battery Cells. *Journal of the Electrochemical Society*, 161(10), pp.A1611–A1617. Available at: http://jes.ecsdl.org/cgi/doi/10.1149/2.0311410jes [Accessed August 26, 2014].

McKenzie, S., 2017. High DCA and Low Water Consumption. In *7th Advanced Automotive Battery Conference Europe*.

Rand, D.A.J. et al., 1996. Valve-regulated lead/acid batteries. *Journal of Power Sources*, 59(1–2), pp.191–197. Available at: http://linkinghub.elsevier.com/retrieve/pii/0378775396023221.

Rosenkranz, C. et al., 2016. Advanced Lead-Acid for 14V Applications Johnson Controls Power Solutions FY2015. In *AABC2016 Europe*. Mainz.

Xu, K., 2004. Nonaqueous liquid electrolytes for lithium-based rechargeable batteries. *Chemical Reviews*, 104(10), pp.4303–4417. Available at: http://pubs.acs.org/doi/abs/10.1021/cr030203g [Accessed May 21, 2013].

Zhang, Z.J. & Ramadass, P., 2012. Lithium-Ion Battery Systems and Technology. In R. A. Meyers, ed. *Encyclopedia of Sustainability Science and Technology*. New York, NY: Springer New York, pp. 319–356. Available at: http://link.springer.com/10.1007/978-1-4419-0851-3 [Accessed May 22, 2013].

Zhao, B. et al., 2015. A comprehensive review of Li 4 Ti 5 O 12 -based electrodes for lithium-ion batteries : The latest advancements and future perspectives. , 98, pp.1–71.